JOURNAL OF CATALYSIS **161,** 319–337 (1996)
ARTICLE NO. 0190

Initial Deactivation of Residue Hydrodemetallization Catalysts

Géraldine Gualda[1] and Slavik Kasztelan[2]

Division Cinétique et Catalyse, Institut Français du Pétrole, BP 311, 92506 Rueil-Malmaison Cedex, France

Received August 9, 1995; revised November 12, 1995; accepted February 2, 1996

Used NiMo/alumina residue hydrodemetallization catalysts with bimodal pore size distribution have been prepared in batch and continuous flow reactors using a Safanyia atmospheric residue. The batch reactor provided used catalysts containing carbon deposits with almost no metal deposits (less than 200 ppm V and 4 to 15 wt% C), whereas the continuous flow reactor provided used catalysts containing both metal and carbon deposits (up to 1.3 wt% V and 11 to 14 wt% C). Used catalyst elemental analysis indicates that within experimental uncertainties the carbon deposits have a density of 1.15 $\pm$ 0.2 g/cm^3 and contain sulfur, nitrogen, and hydrogen with different H/C ratio, the latter depending on both the experimental conditions and the amount of carbon. Characterization of the used catalysts by electron probe microanalysis, secondary ion mass spectrometry, X-ray photoelectron spectroscopy, X-ray diffraction, transmission electron microscopy, and porosimetry show that V and C were well distributed in the catalyst grain in most of the samples and that carbon deposits are best described by three-dimensional patches of amorphous carbon (young coke) which generate pore size restrictions. Both carbon and vanadium have a deactivating effect on toluene hydrogenation, cyclohexane isomerization, and thiophene hydrodesulfurization performed on used catalysts under 6 MPa hydrogen pressure. However, a small amount of vanadium well dispersed inside the catalyst grain has been found to be more deactivating than a large amount of carbon.

INTRODUCTION

Residue hydrodemetallization (HDM) catalysts accumulate large amounts of carbon and metal sulfides deposits and both types of deposits contribute to the catalyst deactivation (1–22). Residue hydrotreaters are operated at constant HDM performance and the deactivation is usually compensated by an increase of reaction temperature. Therefore, the deactivation curve has a so-called S-shape showing a rapid initial deactivation followed by a slow deactivation period and, at the end of the run, a rapid deactivation (23–26).

Carbon is known to accumulate quickly on hydrotreating catalyst surfaces, usually within the first days of a run, until a quasi-steady state is achieved (2, 25, 27–29). This has been often assumed to be the cause of the initial deactivation of residue HDM catalysts based on an analogy with the deactivation of hydroprocessing catalysts by lighter feeds containing no metal contaminants. However, some recent studies suggest that metal deposits may play a major role in the initial deactivation (23, 30). Noticeably, most modeling works of HDM catalyst deactivation take only the metal deposits into account even at the early stage of the deactivation assuming a constant amount of carbon (16, 23, 24, 31, 32) and it is therefore important to determine whether the initial deactivation is mainly due to coke or metal sulfides deposits.

The intermediate slow deactivation period is generally assigned to the metal deposit build up. While the amount of carbon increases only very little, the nature of the carbon species change with time by an ageing process (22).

At the end of the run, the large metal deposits lead to deactivation by pore plugging. However, when the reaction temperature reach the end of run temperature (410°C or more), coke formation is important and may also be the cause of the final deactivation of the catalyst (33).

Studies of catalytic hydrodemetallization have shown that metals contained in the feed (Ni, V) are slowly deposited on the catalyst during a catalytic test leading to contamination of the active phase and to buildup of metal sulfides deposits that ultimately plug the pores of the catalyst (15–17, 23, 24, 34).

Contamination of the NiMoS active phase of these catalysts is viewed as an interaction of metals generated from decomposition of the porphyrinic structures contained in the residue with the NiMoS phase (35–40). Metal deposits are most often viewed as a thick layer of metal sulfides deposited on the surface and especially at the pore mouth. Recent studies indicate, however, that formation of three-dimensional metal sulfide particles is a more realistic model (41–43).

Presence of carbon and metal sulfides deposits makes studies of residue HDM catalysts deactivation by real feed very complex and it is therefore of importance to identify

[1] Present address: Exxon Chemicals, Notre Dame de Gravenchon, France.

[2] To whom correspondence should be addressed. Fax: 33(1) 47.52.60.55. E-mail: slavik.kasztelan@ifp.fr.

0021-9517/96 $18.00

the deactivating effect of each of the deposits. The aim of this work is to determine the importance of the deactivation by coking versus the deactivation by metal deposits of a bimodal macroporous NiMo/alumina residue hydrodemetallization catalyst under real feed operation.

To prepare used catalysts, catalytic tests were designed to obtain coked catalysts with negligible amounts of metal thus minimizing their influence and coked catalysts containing both carbon and small amount of metal deposits well dispersed inside the catalyst grains. The former type of used catalyst was obtained from batch reactor using an atmospheric residue hydrotreated in various operating conditions. To identify key coking parameters, catalyst samples modified by F and Na and feed modified by adding polyaromatics (anthracen or pyrene) were also studied. The latter type of used catalysts were prepared in a continuous flow reactor using the same feed and in similar experimental conditions. Used catalysts were characterized by electron probe microanalysis, secondary ion mass spectrometry, X-ray photoelectron spectroscopy, X-ray diffraction, transmission electron microscopy and porosimetry as well as high pressure (6 MPa) activity tests using model molecules such as toluene hydrogenation, cyclohexane isomerization, and thiophene hydrodesulfurization.

EXPERIMENTAL

Catalysts. A NiO-MoO_3/Al_2O_3 catalyst (NiMo) was prepared by incipient wetness impregnation of a bimodal macroporous alumina support in the form of 1.5 ± 0.5-mm spheres (Rhône-Poulenc, surface area, 140 $m^2\ g^{-1}$; total pore volume, 1.1 cm^3/g) with a solution of ammonium heptamolybdate ($(NH_4)_6Mo_7O_{24} \cdot 4H_2O$ from Merck) and nickel nitrate ($Ni(NO_3)_2 \cdot 6H_2O$ from Prolabo). The catalyst was dried at 100°C and calcined for 4 h at 500°C. The catalyst contained 8.4 wt% Mo and 2 wt% Ni measured by X-ray fluorescence spectroscopy. The main properties of the catalyst are BET surface area of 115 m^2/g, a bulk density of 3.46 g/cm^3, an apparent density of 0.81 g/cm^3, a total pore volume of 0.95 g/cm^3, a mesopore volume (here defined as the volume of pores with diameter smaller than 50 nm) of 0.50 cm^3/g, and a mean mesopore diameter of 17 nm.

Sodium (1 wt%) and fluorine (2.6 wt%) doped NiMo catalysts (samples NiMoNa and NiMoF) were prepared by incipient wetness impregnation of sodium nitrate and ammonium hydrogen fluoride, respectively, and then dried at 150°C and calcined at 450°C, 2 h, One batch of NiMo catalyst was impregnated with 5.4 wt% quinoline before presulfidation (sample NiMoQ).

Prior to use in batch reactor, these catalysts were presulfided using the SULFICAT process (44). The amounts of sulfur deposited were chosen to reach an atomic ratio $S/(Mo + Ni) = 2$. For example, the presulfided and aromatic solvent extracted NiMo catalyst contained 6.4 wt% S and 2.9 wt% C, the latter resulting from the SULFICAT process itself.

TABLE 1

Properties of Safanyia Crude Atmospheric Residue

Metals content (wt ppm)	Ni, 25; V, 81
Heteroatom content (wt%)	S, 4.1; O, 0.9; N, 0.25
C, H (wt%)	C, 84.3; H, 11.3
Specific gravity	0.977
Conradson carbon (wt%)	15.5
C7-asphaltens (wt%)	7.2
Resins (wt%)	5.1
Viscosity at 100°C (Cst)	200
Distillation (°C)	
IBP	284
10%	470
50%	555

Batch reactor tests. Catalytic tests were performed in a 500-ml stainless steel batch reactor under hydrogen pressure using 50 g of presulfided catalyst and 125 g of Safanyia atmospheric residue (SAR). The main properties of the SAR feed are reported in Table 1. These quantities correspond to approximately 1/3 of the volume of the reacting mixture occupied by the catalyst and 2/3 by the surnageant liquid. Good mixing was obtained by using sea helix rotating at 650 rpm and positioned at 1/3 of the height of the reacting mixture from the bottom of the reactor. The experimental conditions were total pressure, 2 to 15 MPa; reaction temperature, 370 to 420°C; contact time, 0 to 3 h; and hydrogen flow rate, 30 liters/h. The experimental conditions mentioned in the text as being "reference conditions" were 12 MPa total pressure, 390°C, and 1 h contact time. The catalyst/oil mass ratio of 0.4 leads to a reaction time of 2.5 h for a 1 h contact time and a H_2/Oil volume ratio of 430 Nl/liter for a 30 liter/h hydrogen flow rate.

One drawback of the batch reactor is clearly the existence of a period of time were the feed and catalyst are in contact at a temperature lower than the reaction temperature but allowing catalytic reactions to start. In this work, the contact time zero was set up at 80 min after starting the heating ramp from room temperature to the reaction temperature (between 370 and 420°C). Then, after loading the presulfided catalyst and the feed, the unit was pressurized and checked for leaks and the temperature was increased to reach the reaction temperature chosen in 80 min by changing the heating rate. The mixing was started gently at 80°C. One important feature of the use of a batch reactor is that the catalyst/oil ratio determines the maximum amount of metal deposited on the catalyst which is 203 wt ppm V + 62 wt ppm Ni in our experiments.

Series of tests were performed with the reference NiMo catalyst by changing one operating parameter at a time such as the contact time (samples CT), the pressure (samples *P*),

and the temperature (samples *T*) starting with a fresh catalyst load. The doped catalysts (samples NiMoF, NiMoNa, and NiMoQ) as well as the macroporous alumina support of the NiMo catalyst (sample *S*) were also tested in the reference conditions previously defined. Experiments were also made with the reference catalyst and the SAR feed containing 20 wt% anthracen (samples AN1.2, AN2) or 20 and 40 wt% pyren (samples PY20 and PY40). For these latter tests the same catalyst/oil mass ratio = 0.4 have been kept and the contact time was computed relative to the amount of SAR feed in the mixture.

Continuous flow reactor tests. Catalytic tests were performed in a high pressure fixed bed continuous flow "Catatest" unit from VINCI Technologies, using the SAR feed. The experimental conditions employed were total pressure, 8 MPa; reaction temperature, 380°C; LHSV, 1 h^{-1}; H_2/HC, 1000 Nl/liter; and 80 cm^3 catalyst. The catalyst was loaded in the oxide form and sulfided at 350°C, 4 h, LHSV = 1 h^{-1}, H_2/HC = 400 Nl/liter with a gas oil spiked with 2 wt% dimethyldisulfide. One series of coked NiMo catalysts was prepared by varying the length of the time on stream from 6 to 240 h on stream (samples TS). Before recovering the used catalyst, the unit was washed by gas oil at 250°C for 24 h.

Feed and effluent analysis. S, Ni, V contents of the effluents were measured by X-ray fluorescence. N contents were measured by chemiluminescence. Asphalten is defined as the fraction soluble in hot toluene and insoluble in *n*-heptane. Resin is defined as the fraction soluble in hot toluene and insoluble in pentane minus the Asphalten fraction. Simulated distillation was determined up to 575°C by a HP5880 gas chromatograph equipped with a DEXIL 300 column and a FID. From these data the various conversions (HDX) determined were hydrodesulfurization (HDS), hydrodenitrogenation (HDN), hydrodevanadization (HDV), hydrodenickelization (HDNi), hydrodeasphaltenization (HDAs), hydroderezination (HDRe) and hydroconversion into 350°C minus fraction (HDC).

Model molecules tests. Toluene hydrogenation, cyclohexane isomerization into methylcyclopentane, and thiophene hydrodesulfurization tests were performed in a high pressure fixed bed continuous flow "Catatest" unit from VINCI Technologies. Toluene hydrogenation and cyclohexane isomerization were determined simultaneously at 6 MPa, 350°C, LHSV = 2 h^{-1}, H_2/HC = 450 Nl/liter, and 40 cm^3 catalyst. The liquid feed was composed of toluene (20 wt%), thiophene (2 wt%), and cyclohexane (78 wt%). In these conditions thiophene was found completely hydrogenated into butane and H_2S as checked by GC analysis.

The toluene hydrogenation test was followed by a thiophene hydrodesulfurization test performed at 6 MPa, 220°C, LHSV = 2 h^{-1}, H_2/HC = 300 Nl/liter. The liquid feed was composed of dimethyldisulfide (1 wt%), thiophene (2 wt%), and *n*-heptane (97 wt%). The liquid products of the reactions were analyzed by gas chromatography using a 50-m CPSIL8 column at 60°C and a flame ionization detector. First-order kinetic laws were used to compute the hydrogenation, isomerization, and hydrodesulfurization rate coefficients in mol/g/h.

Prior catalytic tests, the samples were sulfided *in situ* by 2 wt% dimethyl-disulfide in cyclohexane at 6 MPa, from room temperature to 350°C with a ramp of 2°C/min followed by a 4 h stand at 350°C.

Used catalysts analysis and characterization. The used catalyst recovered were washed with toluene in a Soxhlet, stored in purified toluene, and dried before analysis. C, H, S, and N elemental analyses were performed by combustion (Dumas method) using a Carlo Erba apparatus. The coke is therefore defined in this work as being the carbon content of used catalysts washed by hot toluene. Metal contents were measured by X-ray fluorescence (XRF) and fluorine and sodium contents by atomic adsorption. The hydrogen content of coke was determined by difference between the hydrogen content measured for the used catalyst and the hydrogen content measured for the fresh NiMo catalyst (0.6 wt%) or the support (0.6 wt%).

Textural analysis of all of the fresh and used samples were performed by mercury porosimetry, mercury picnometry, helium picnometry, and BET surface area measurements. Prior to analysis the samples were heated at 300°C under helium to remove volatile hydrocarbons.

Electron probe microanalysis (EPMA) of used catalysts was performed with a Camebax electron microprobe to measure the radial concentration profile of the metals and carbon in the catalyst spheres. For EPMA, five spheres were covered by a gold film and then embedded in a resin. Then the pieces of resin were polished before recording the radial concentration profiles of Mo, S, V, C, and Al and reporting the mean radial concentration profile of the five spheres.

Carbon radial concentration profile of the used catalysts containing less than 10 wt% carbon were measured by secondary ion mass spectroscopy (SIMS) on a Cameca IMS 3F apparatus using the O_2^+ primary ion and recording the $^{24}C_2^-$ ion signal and, to allow determination of the edge limit of the sphere, the oxygen ion $^{16}O^-$ ion signal. Sample preparation was performed as for the EPMA measurements.

X-ray diffraction (XRD) analyses were performed with a Siemens D501 automatic diffractometer on powdered samples.

X-ray photoelectron spectroscopy (XPS) analysis were performed with a Kratos XSAM800 spectrometer using an Al$K\alpha$ source (1486.6 eV). Binding energies are reported relative to the Al 2p peak of the alumina support (74.6 eV) with C 1s at 285 eV. A theoretical curve has been computed for the variation of the C 1s over Al 2p intensity ratio versus the carbon content in the case of a uniform coverage according to the model of Kerkhoff and Moulijn (45) and using

the $\sigma_{C\,1s}$ and $\sigma_{Al\,2p}$ cross sections reported by Scofield (46):

$$\frac{I_{C\,1s}}{I_{Al\,2p}} = \frac{\sigma_{C\,1s}}{\sigma_{Al\,2p}}\left(\frac{Ek_{C\,1s}}{Ek_{Al\,2p}}\right)^{1.77}\left(\frac{[C]}{[Al]}\right)_{at.} \quad [1]$$

$$\frac{I_{C\,1s}}{I_{Al\,2p}} = 1.47\left(\frac{[C]}{[Al]}\right)_{at.}. \quad [2]$$

Samples analyzed by transmission electron microscopy (TEM) were pretreated in the same manner as described for the XPS measurements, but were transferred to the microscope undried to avoid contact of the surface with air. TEM images were recorded using a JEOL 100 CX instrument.

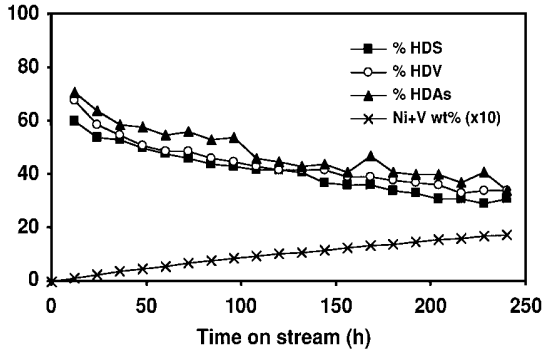

FIG. 1. HDS, HDV, HDAs, and metal content deposited versus time on stream during hydrotreatment of Safanyia atmospheric residue at 8 MPa, 380°C, LHSV = 1 h^{-1}.

RESULTS

Results from the catalytic tests and actual values for the S, N, and H content of used catalysts are reported in Table 2 for all of the used catalysts prepared. These used catalysts have been given symbols composed of the symbol of the series (TS, P, T, CT, or S) followed by the value of the parameter modified.

Effect of time on stream in continuous flow reactor (TS series). A first set of catalytic tests was performed in continuous flow reactor. The experimental conditions and, in particular, a low pressure were chosen to favor carbon deposition and minimize metal deposition, i.e., the HDM. The operating conditions were 8 MPa, 380°C, LHSV = 1 h^{-1}, and to obtain a series of used catalysts containing increasing amounts of carbon, several tests were performed by increasing the time on stream (TS) from 6 to 240 h starting each time with a fresh catalyst.

Figure 1 shows the variation of HDS, HDV, and HDAs and the increase of the cumulated amount of Ni + V versus time on stream for the longest test performed in this work, i.e., 240 h. Deactivation of the HDS function versus time on stream appears exponential as a linear relationship has been found when the HDS activity (computed using a 1.5 order according to Ref. 47) is plotted against the log of time on stream. Similar behavior were found for the other reactions.

Table 2 shows that the HDX conversions followed the decreasing order HDAs > HDV ≥ HDS > HDN > HDRe ≥ HDNi which confirms that deasphaltenization, HDV, and HDS are easier than HDN and HDNi. Metal contents computed from the HDV and HDNi increased up to 1.7 wt% relative to the fresh catalyst. Such an amount is small compared to the large metal retention capacity of this type of catalysts but too large to neglect the deactivating effect of metal deposits.

Figure 2 shows that carbon is very quickly deposited onto the catalyst surface, starting at a level of about 11 wt% after 6 h on stream to reach an almost steady level at 14 wt% after 240 h on stream. Also reported in Fig. 2 is the H/C ratio of the carbon deposits computed by subtracting the hydrogen content of the fresh catalyst (0.6 wt%), a standard procedure, from the total amount of hydrogen of the used catalyst. In Fig. 2, it can be observed that when the time on stream increases, the H/C ratio decreases from 0.84 to 0.61 and the carbon content increases slowly. This indicates a slow transformation of the carbon deposit with time toward a more dehydrogenated form.

Effect of contact time in batch reactor (CT series). In order to minimize the amount of metal deposited while obtaining coked catalysts, tests in a batch reactor were performed. The CT series of used samples was obtained at 390°C, 12 MPa, and 30 liters H_2/h hydrogen flow rate, by changing the contact time from 0 to 3 h. As shown in Table 2, all HDX conversions increased as contact time increased. Conversion levels were high with HDS, HDV, and HDAs at more than 60%, indicating that at high contact time the feed was deeply transformed. From the activity data, determination of the orders of reaction have been attempted for all reactions but no linear relationships could be obtained with orders included between 0.5 and 2, indicating the existence of a complex kinetic behavior of the system.

The used catalysts contained between 150 and 200 ppm V, a low level than can be neglected. Figure 3 shows that the carbon content decreases with increasing contact time. At zero contact time, sample CT0 contains the higher amount of carbon. This carbon is generated during the heating time. The decrease in the carbon content as the contact time increases is related to the increase of the purification of the feed. This indicates that the carbon initially deposited onto the catalyst surface is transformed as the feed is purified. In Fig. 3, the H/C ratio varies from 0.8 to 1.2 and goes through a maximum which can be interpreted by a competition between the formation of a more hydrogenated carbon deposit as the feed gets purified and the tendency to form a more dehydrogenated residual carbon deposit after long contact time, an effect which can be related to the aging of the carbon deposits. The H/C ratio is, however, relatively

TABLE 2

Batch and Continuous Flow Tests Results and Used Catalysts Compositions

Sample		HDS (wt%)	HDN (wt%)	HDV (wt%)	HDNi (wt%)	HDAs (wt%)	HDRe (wt%)	HDC (wt%)	V (ppm[a])	C (wt%)	H (wt%)	N (wt%)	S (wt%)
Continuous flow, time on stream series (catalyst, NiMo oxide sulfided by GO + DMDS)													
TS6	6 h	63.3	26.8	71.9	25.4	73.4	32.8	—	600[b]	11.4	1.4	0.3	5.6
TS12	12 h	59.4	25.3	67.6	21.7	71.1	26.8	—	1,080	12.1	1.4	0.3	5.8
TS24	24 h	53.8	13.2	58.5	11.4	63.7	17.9	—	2,000	12.0	1.4	0.3	5.7
TS72	72 h	46.4	13.9	49.2	12.6	55.8	9.9	—	5,200	13.4	1.4	0.3	5.5
TS120	120 h	41.5	14.0	42.8	6.7	45.0	12.0	—	7700[b]	13.6	1.3	0.3	6.1
TS240	240 h	30.4	3.8	34.8	9.2	34.2	6.4	—	13,000[b]	13.7	1.3	0.3	5.6
Batch, contact time series (catalyst, NiMo presulfided, 12 MPa, 390°C)													
CT0	0 h	60.3	19.5	83.0	43.3	85.7	50.6	5.5	168	6.4	1.1	0.2	6.0
CT0.1	0.1 h	68.1	30.3	92.6	60.7	94.3	77.5	5.4	188	6.4	1.1	0.2	5.7
CT0.25	0.25 h	77.3	29.9	95.6	80.5	95.6	91.1	5.5	194	6.2	1.1	0.2	5.9
CT0.5	0.5 h	85.5	42.2	98.5	88.0	96.5	91.2	8.9	199	5.2	1.1	0.2	5.5
CT1 = T390 = P12	1 h	92.4	46.5	98.3	82.4	96.8	92.1	12.0	199	5.2	1.1	0.1	5.4
CT1.5	1.5 h	96.9	62.2	98.8	85.4	97.5	94.6	16.0	200	4.6	1.0	0.1	5.5
CT2	2 h	98.5	62.7	99.5	92.4	98.0	95.8	19.5	201	4.2	0.9	0.1	4.9
CT3	3 h	99.6	68.9	98.8	91.7	98.9	98.2	28.0	200	4.1	0.9	0.2	5.1
Batch, contact time series (catalyst, support presulfided, 12 MPa, 390°C)													
S-CT1	1 h	21.6	19.5	60.1	48.2	39.4	49.9	10.2	122	9.5	1.1	0.1	0.84
S-CT2	2 h	25.3	26.5	74.9	77.8	61.5	57.3	19.1	152	10.7	1.0	0.2	0.88
Batch, temperature series (catalyst, NiMo presulfided, 12 MPa, CT = 1 h)													
T370	370°C	86.8	36.9	95.5	62.4	91.5	81.4	6.0	193	6.1	1.2	0.2	5.2
T380	380°C	91.9	44.7	97.9	74.7	94.8	86.7	7.5	198	5.5	1.2	0.2	5.2
T400	400°C	96.9	42.0	98.2	97.9	97.1	93.4	16.0	199	4.9	1.1	0.2	5.1
T410	410°C	94.3	50.7	98.4	99.0	99.2	98.4	27.0	199	4.9	1.0	0.2	5.5
T420	420°C	97.6	75.9	99.9	99.9	99.1	98.4	43.0	202	4.5	1.0	0.2	5.5
Batch, pressure series (catalyst, NiMo presulfided, CT = 1 h, 390°C)													
P2	2 MPa	66.8	26.1	89.0	51.4	66.9	80.2	14.1	180	10.1	1.1	0.2	5.7
P3	3 MPa	74.0	25.3	88.8	65.8	63.5	85.0	11.9	180	9.7	0.9	0.2	5.6
P5	5 MPa	85.7	38.5	93.6	78.5	85.0	71.0	13.0	190	8.0	0.9	0.2	5.6
P5–CT2	5 MPa, 2 h	91.1	43.9	96.3	80.1	—	—	—	195	7.0	1.2	0.2	5.4
P7	7 MPa	86.4	39.7	94.5	79.9	90.1	82.2	10.7	191	6.9	1.1	0.2	5.7
P9	9 MPa	89.7	44.4	97.7	81.0	97.4	88.6	13.0	198	6.6	1.1	0.2	6.0
P11	11 MPa	92.2	53.2	97.3	79.1	97.5	91.8	11.7	197	5.2	1.0	0.1	5.6
P13	13 MPa	92.4	51.8	98.9	79.7	98.3	93.8	12.0	200	4.9	1.1	0.2	5.7
P15	15 MPa	93.7	67.9	98.9	83.2	98.7	97.5	11.5	200	4.0	1.1	0.2	5.6
Batch, doped catalyst series (presulfided catalysts; exp. conditions, 5 MPa, 390°C, CT = 1 h)													
NiMoF	2.6 wt% F	84.4	38.6	97.9	86.8	89.3	76.0	9.7	198	8.2	0.9	0.4	4.7
NiMoNa	1.05 wt% Na	76.5	22.7	92.4	74.0	82.7	62.0	11.1	187	6.5	0.9	0.2	5.9
NiMoQ	5.4 wt% Q	74.4	16.7	92.9	82.3	—	—	—	188	8.1	1.1	0.2	6.1
Batch, anthracen series (catalyst, NiMo presulfided; exp. conditions, 12 MPa, 390°C, 20 wt% anthracen)													
AN1.20	CT = 1.2 h	95.1	58.2	98.0	90.1	—	—	—	198	3.7	1.0	0.1	5.6
AN2	CT = 2 h	98.3	63.8	99.0	95.0	—	—	—	200	3.3	0.9	0.2	5.5
Batch, pyren series (catalyst, NiMo presulfided; exp. conditions, 5 MPa, 390°C, CT = 2 h)													
PY20	20 wt% Pyren	92.8	50.8	97.9	90.1	—	—	—	198	5.5	1.0	0.2	5.9
PY40	40 wt% Pyren	93.2	61.3	97.2	88.4	—	—	—	197	5.8	0.9	0.1	5.2

[a] Computed from HDV on a fresh catalyst basis.
[b] Measured by X-ray Fluorescence.

high and can be assigned to alkylated polyaromatic compounds containing two or three rings. This H/C ratio corresponds also to "young and moderately aged coke," whereas "aged coke" would have a H/C ratio from 0.4 to 0.6 (48).

The alumina support of the NiMo catalyst was also tested in the same conditions at contact times 1 and 2 h (samples S-CT1 and S-CT2, respectively) to get some insight on the effect of the support on the carbon deposition. The HDX activities of the alumina support alone are not negligible, as shown in Table 2, indicating that thermal processes have an important contribution when there is no active phase as reported recently (49).

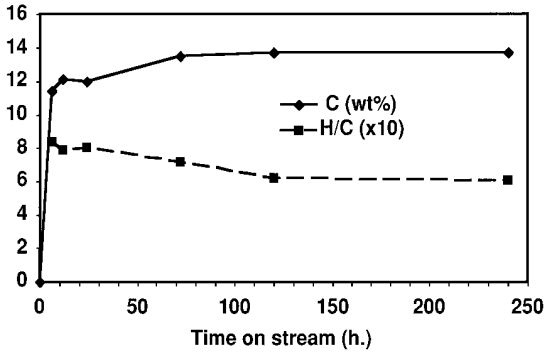

FIG. 2. Carbon content and H/C molar ratio of used catalysts versus time on stream from continuous flow tests.

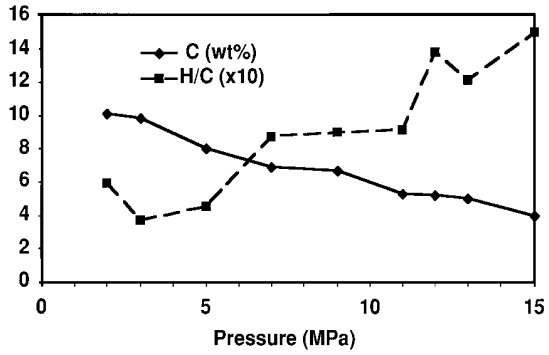

FIG. 4. Carbon content and H/C molar ratio of used catalysts versus pressure from batch reactor tests.

The amount of carbon deposited on the alumina support is clearly larger than for the NiMo catalyst, as shown in Fig. 3. The H/C ratio is, however, smaller than the H/C ratio of the coked NiMo catalysts, indicating that the carbon deposited on the support alone is more dehydrogenated than the carbon deposited on the NiMo catalyst. All this information indicates that in presence of an active phase the amount of carbon is limited and coke is also more hydrogenated (49).

Effect of pressure in batch reactor (P series). The effect of increasing the pressure from 2 to 15 MPa at 390°C, 1 h contact time, and 30 liters H_2/h hydrogen flow rate was to increase all of the HDX conversions, as shown in Table 2 (samples P20 to P150). Above 12 MPa, however, the HDS, HDNi, and HDC reached a plateau. Carbon contents decreased and the H/C ratio increased when pressure increased, as shown in Fig. 4. This again clearly shows the beneficial effect of favoring the hydrogenation to limit the amount of carbon deposits.

At 5 MPa pressure, one test was performed with a 2 h contact time (P50–CT2). The results from the elemental analysis of the used catalyst confirmed the decrease in the carbon content with increasing contact time, as already observed for the CT series (Table 2).

Effect of temperature in a batch reactor (T series). The effect of increasing the reaction temperature from 370 to 420°C at 12 MPa, 1 h contact time, and 30 liters H_2/h hydrogen flow rate (samples T370 to T420) was to increase all of the HDX conversions. Quite surprisingly the carbon content of the used catalysts decreases, whereas the H/C ratio seems to go through a maximum at 390°C as shown in Fig. 5. This suggests that by increasing the reaction temperature up to 390°C the coke is hydrogenated (kinetic regime) and desorbed from the catalyst surface, whereas at higher temperature dehydrogenation is favored (thermodynamic regime).

Modification of the catalyst acidity (NiMoNa, NiMoF, and NiMoQ samples). The NiMo catalyst acidity was modified by adding sodium or quinoline to neutralize the surface acidity and fluorine to increase the surface acidity. Catalytic tests with the Safanyia atmospheric residue were performed in batch reactor at 5 MPa, $T = 390$°C, 1 h contact time, and 30 liters H_2/h hydrogen flow rate. The results reported in Table 2 indicate that sodium and quinoline have a deactivating effect for most reactions considered, whereas fluorine tends to increase catalytic performances. The carbon content of the used catalyst is not influenced by quinoline or fluorine but is clearly decreased by presence of sodium.

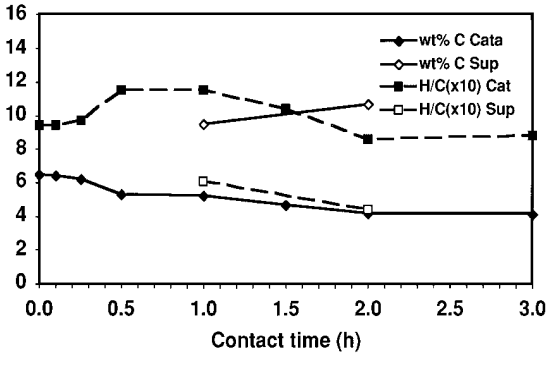

FIG. 3. Carbon content and H/C molar ratio of used catalysts versus contact time from batch reactor tests.

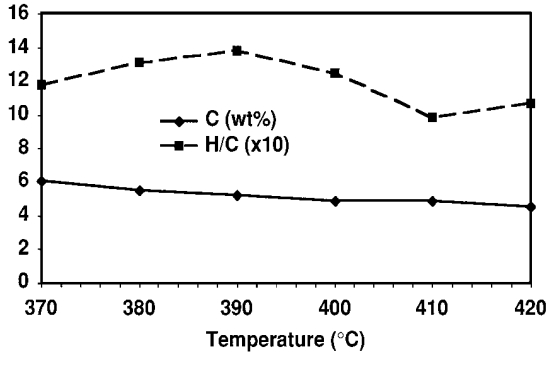

FIG. 5. Carbon content and H/C molar ratio of used catalysts versus temperature from batch reactor tests.

Effect of feed additives (Series AN and PY). To investigate the influence of the feed on the coking behavior of the catalyst, anthracen or pyren was added to the feed in a large proportion. For anthracen addition, the experimental conditions for the tests in batch reactor were 12 MPa, $T = 390°C$, 2 h contact time, and 30 liters H_2/h hydrogen flow rate. In these conditions anthracen hydrogenation is not thermodynamically limited (50). A large hydrogen consumption was observed with an outlet hydrogen flow rate of 20 liters H_2/h. Mass spectrometry analysis of the effluents indicated that anthracen was completely transformed (within the experimental uncertainties) and hydrogenated forms such as octahydroanthracen (35 wt%), decahydroanthracen (7 wt%), and perhydroanthracen (58 wt%) were detected.

The effect of adding anthracen on the catalytic properties is minor (AN series in Table 2). However, anthracen addition tends to decrease the amount of carbon deposited. As anthracen is deeply hydrogenated it is likely that its contribution to the coking is minor; hence the decrease of the carbon content on the used catalyst suggests that anthracen limit the coking of the catalyst by the SAR feed although the hydrogen consumption was larger.

A test was also performed with pyren added to the feed under the following experimental conditions: 5 MPa, $T = 390°C$, 2-h contact time, 30 liters H_2/h hydrogen flow rate. For these tests, the low pressure was chosen to have a thermodynamically limited hydrogenation reaction (51). A calculation of pyren hydrogenation level in our experimental conditions using the values given in Ref. 51 for the equilibrium pyren–dihydropyren led to 29% of hydrogenated forms. Mass spectrometry analysis of the effluent indicated that 25 wt% of the pyren was hydrogenated, in good agreement with the calculated value. The main identified product were dihydropyrene (15 wt%), hexahydropyrene (9 wt%), and traces of perhydropyrene. These products are clearly those encountered in the literature on pyren hydrogenation (52). In addition, the contact time had no effect on the product distribution, indicating the presence of a thermodynamic limitation.

The presence of pyren in the feed tends to increase the HDX conversion and in particular the HDN. Carbon contents of used catalysts decreased a little, although pyren may also contribute to the coking of the catalyst.

Elemental analysis of used catalysts. All of the used catalysts have been washed with toluene and their C, S, N, and H contents determined and reported in Table 2. Variations in sulfur content and nitrogen content in all of the used catalysts versus the carbon content are reported in Figs. 6 and 7, respectively. Although these catalysts were obtained from many different experiments and within experimental uncertainties, some general tendencies appear in these figures. In Fig. 6, the sulfur content increases linearly with the carbon content and the slope of the straight line led to a mean value for the sulfur content in the carbon deposits of $S/C = 0.035 \pm 0.01$.

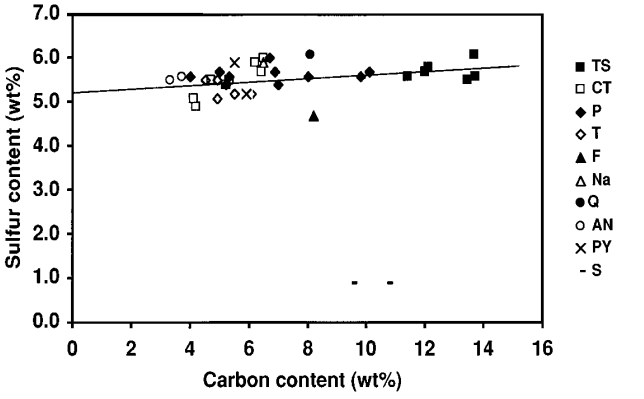

FIG. 6. Actual sulfur versus carbon content for the various sets of used catalysts.

The fresh NiMo catalyst contains no nitrogen and upon carbon deposition, the nitrogen content increases with carbon content, as found in Fig. 7. Although there is a large scattering of the data in Fig. 7, the slope of the straight line plotted allowed evaluation of the approximate nitrogen content of the coke deposits with a N/C ratio of 0.02 ± 0.01. These nitrogen contents of used catalysts are in line with values reported in the literature (4, 53–59).

The hydrogen content of the used catalysts plotted versus the carbon content led surprisingly also to a monotonous relationship, although these catalysts where obtained in different conditions. The corrected H/C ratio for all of the used catalysts have been plotted versus the carbon content in Fig. 8 and it is found that the H/C ratio decreases when the C content of the catalyst increases. Plotting the corrected H/C ratio versus 1/C led to a linear tendency with a rather large scattering of the data.

Textural characterization of used catalysts. Table 3 summarizes the results from the textural characterization of all

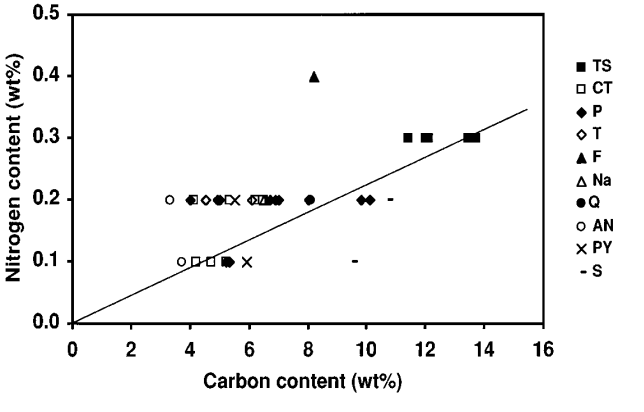

FIG. 7. Actual nitrogen versus carbon content for the various sets of used catalysts.

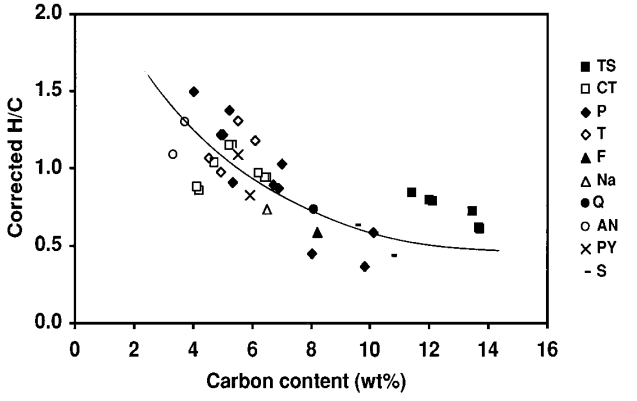

FIG. 8. Corrected H/C ratio versus carbon content for the various sets of used catalysts.

of the used catalysts obtained from batch and continuous flow reactor experiments. From the data in Table 3, it is shown that the bulk density of the used catalysts (ds_u) decreases monotonously when the carbon content increases and a linear relationship is found when the reciprocal bulk density of the used catalyst is plotted against the carbon content as shown in Fig. 9. Although there is some scattering of the data at low carbon content, at zero carbon content the straight line passes through the value of the bulk density of the fresh oxide catalyst. It can be demonstrated that there is a linear relationship between the reciprocal of the bulk density of the used catalyst and the carbon content (C in wt%) depending on the coke density ds_c and assuming no occluded volume or an occluded volume independent of the carbon content (see Appendix I). This linear relationship (formula [I.10] in Appendix I) is verified in Fig. 9 and from the slope of the straight line; the value of 1.15 ± 0.2 g/cm^3 is calculated as the mean value of the coke bulk density.

The carbon deposits may plug some pores and generate some occluded volume, although the rather large mean mesopore diameter of the catalyst and the measurement of pore volumes using helium make such a hypothesis not very likely. From the total pore volumes of the fresh and used catalysts, and using the coke density to compute the volume of coke, the occluded volume can be estimated (see Appendix I, formula [I.11]). The fractions of the catalyst pore volume occupied by coke (vc), occluded (voc) and still accessible (vac), have been computed and are reported in Table 3. The occluded volume remains small and within uncertainties for all of the samples. The volume of carbon is also small compared to the total pore volume.

Other textural analyses have been performed to shed some light on the mode of carbon deposition inside the grain. Analysis of the surface area measurements was inconclusive with little variation of surface area between all the samples as shown in Table 3. Pore size distribution of the fresh and used catalysts were determined and the distribution of pore diameters in the range 1 to 500 nm versus the carbon content is reported in Fig. 10. In this figure, it appears clearly that despite the small volume occupied by the carbon deposits there is a large change in the mean pore diameter toward smaller sizes. BET surface area and pore volume measurements allow the computation of the mean mesopore diameter (MPD), assuming a cylindrical pore model using the relationship

$$\mathrm{MPD} = 4000\frac{V_\mathrm{m}}{A}\ (\text{in nm}), \qquad [3]$$

with A representing the BET surface area and V_m the mesopore volume defined here as volume of pores with a diameter smaller than 50 nm.

For each of the used catalysts, the mesopore volume has been determined and the mean mesopore diameter computed. The variation of the mean mesopore diameter versus the carbon content of the used catalysts is plotted in Fig. 11. Although there is some scattering of the data, a monotonous but steep decrease of the mean mesopore diameter is found. Noticeably, used catalysts with 10 to 14 wt% C, in particular from the time on stream series TS, have mesopore sizes drastically reduced although the carbon content remains moderate. For such a carbon loading, the mean mesopore diameter is about 3 nm, indicating the creation of severe pore restrictions although the volume occupied by the carbon is no more than 15% of the total pore volume (Table 3) or 28% of the mesopore volume.

Physico-chemical characterization of used catalysts. The EPMA vanadium radial concentration profile of sample TS120 obtained in a continuous flow reactor for a time on stream of 120 h and containing 0.77 wt% V is shown in Fig. 12a. The V radial concentration profile is almost flat, indicating a very good accessibility of the feed to all of the catalyst volume and the absence of diffusional limitations in our experimental conditions. Similar results were found for the other samples.

The EPMA carbon radial concentration profile of the sample TS240 obtained in continuous flow reactor for a time on stream of 240 h and containing 13.7 wt% C and 1.3 wt% V is shown in Fig. 12b. To detect carbon with a good sensitivity, the sample containing the largest amount of carbon had to be chosen. The EPMA carbon radial concentration profile shows also that for this sample the carbon is also well distributed in the total catalyst volume.

To determine the carbon radial concentration profile of samples with lower carbon contents, SIMS analyses were performed on four samples of the P series. Figure 13 shows the carbon radial concentration profile of the fresh catalyst and the P2, P5, P9, and P15 samples containing 10.1, 8, 6.6, and 4 wt% C, respectively. In these experiments the catalyst spheres were embedded in a resin and the limit of the catalyst sphere was determined by the oxygen signal as shown

TABLE 3

Textural Properties of Used Catalysts and Supports

Sample		C (wt%)	V (ppm[a])	A (BET surf., m^2/g)	ds_u (Bulk dens., g/cm^3)	dg (App. dens., g/cm^3)	TPV (calc, cm^3/g)	v_{ac} (accessible volume, %)	v_c (volume of carbon, %)	v_{oc} (occluded volume, %)
Continuous flow, time on stream series (catalyst, NiMo oxide sulfided by GO + DMDS)										
TS6	6 h	11.40	600[b]	120	2.76	0.96	0.68	81	12	7
TS12	12 h	12.10	1080	120	2.75	0.99	0.65	78	13	10
TS24	24 h	12.00	2000	120	2.75	0.98	0.66	79	13	9
TS72	72 h	13.45	5200	120	2.72	1.08	0.56	68	14	17
TS120	120 h	13.65	7700[b]	121	2.72	1.07	0.57	69	15	16
TS240	240 h	13.70	13000[b]	129	2.74	1.11	0.54	66	15	20
Batch, contact time series (catalyst, NiMo presulfided, 12 MPa, 390°C)										
CT0	0 h	6.45	168	108	3.00	0.91	0.77	87	6	7
CT0.1	0.1 h	6.40	188	123	3.02	0.90	0.78	88	6	6
CT0.25	0.25 h	6.15	194	109	3.07	0.89	0.80	90	6	4
CT0.5	0.5 h	5.25	199	113	3.15	0.85	0.86	96	4	0
CT1 = T390 = P12	1 h	5.20	199	118	3.11	0.87	0.83	92	5	3
CT1.5	1.5 h	4.65	200	113	3.22	0.88	0.83	92	4	4
CT2	2 h	4.20	201	108	3.23	0.87	0.84	93	4	3
CT3	3 h	4.10	200	104	3.20	0.90	0.80	88	4	8
Batch, contact time series (catalyst, support presulfided, 12 MPa, 390°C)										
S-CT1	1 h	9.5	122	127	2.86	0.77	0.92	93	7	0
S-CT2	2 h	10.7	152	125	2.90	0.79	0.89	91	9	0
Batch, temperature series (catalyst, NiMo presulfided, 12 MPa, CT = 1 h)										
T370	370°C	6.10	193	104	2.92	0.87	0.81	91	6	3
T380	380°C	5.50	198	105	3.01	0.94	0.73	82	5	13
T400	400°C	4.90	199	110	3.16	0.88	0.82	91	5	4
T410	410°C	4.90	199	99	3.11	0.92	0.77	85	5	10
T420	420°C	4.50	202	103	3.10	0.86	0.84	93	4	3
Batch, pressure series (catalyst, NiMo presulfided, CT = 1 h, 390°C)										
P2	2 MPa	10.10	180	109	2.87	0.96	0.69	82	10	8
P3	3 MPa	9.75	180	104	2.89	0.97	0.68	80	10	10
P5	5 MPa	8.00	190	108	3.01	0.91	0.77	88	8	4
P5-CT2	5 MPa, 2 h	7.00	195	127	3.06	0.88	0.81	92	7	1
P7	7 MPa	6.90	191	108	3.02	0.89	0.79	90	7	3
P9	9 MPa	6.65	198	115	3.06	0.92	0.76	86	7	7
P11	11 MPa	5.25	197	115	3.10	0.91	0.78	87	5	8
P13	13 MPa	4.95	200	109	3.21	0.90	0.80	89	5	6
P15	15 MPa	4.00	200	120	3.21	0.91	0.79	87	4	9
Batch, doped catalyst series (presulfided catalysts; 5 MPa, 390°C, CT = 1 h)										
NiMoF	2.6 wt% F	8.2	198	125	2.97	0.95	0.72	82	8	9
NiMoNa	1.05 wt% Na	6.5	187	124	3.06	0.93	0.75	85	6	9
NiMoQ	5.4 wt% Q	8.1	188	110	2.97	0.96	0.70	87	8	11
Batch, anthracen series (catalyst, NiMo presulfided; 12 MPa, 390°C, 20 wt% anthracen)										
AN1.20	CT = 1.2 h	3.70	198	127	3.23	0.88	0.83	91	4	6
AN2	CT = 2 h	3.30	200	122	3.29	0.86	0.86	94	3	3
Batch, pyren series (catalyst, NiMo presulfided; 5 MPa, 390°C, CT = 2 h)										
PY20	20 wt%	5.50	198	128	3.15	0.88	0.82	92	5	3
PY40	40 wt%	5.85	197	120	3.13	0.94	0.74	84	6	11

[a] Computed from HDV on a fresh catalyst basis.
[b] Measured by X-ray Fluorescence.

for the P9 sample (Fig. 13, profile d). In this series of used catalysts, the carbon radial concentration profiles appears almost flat at low carbon content up to 6.6 wt%. At higher carbon content, a nonuniform radial carbon distribution, U-shaped, is observed, suggesting the appearance of diffusional limitations. Recent determinations of carbon radial concentration profile on spent hydrotreating catalysts using nuclear microprobe analysis indicate also uniform and U-shaped concentration profiles through the catalyst grains (53). Note that in Fig. 13 the nonuniform radial distribution

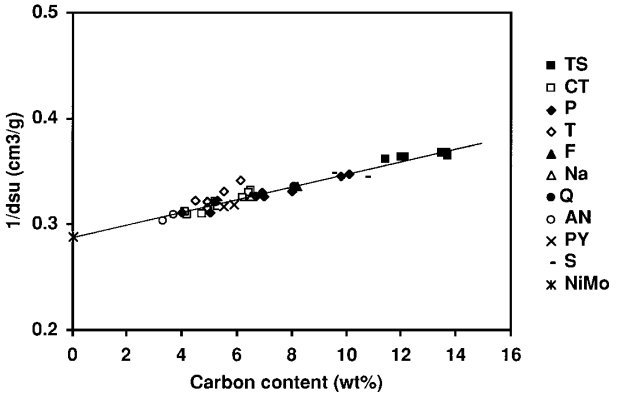

FIG. 9. Reciprocal of bulk density versus carbon content for all of the used catalysts and supports.

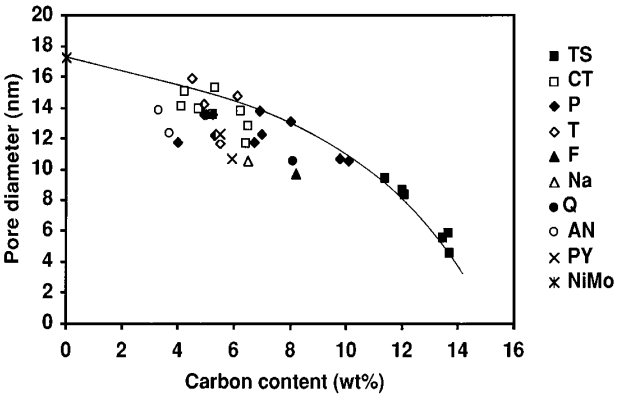

FIG. 11. Mean mesopore diameter versus carbon content for all of the used catalysts.

of carbon increases when the carbon content increases or the pressure decreases.

X-ray diffraction analysis of the used samples kept in toluene and dried before analysis showed no evidence of the 002 line characterizing graphitic structure.

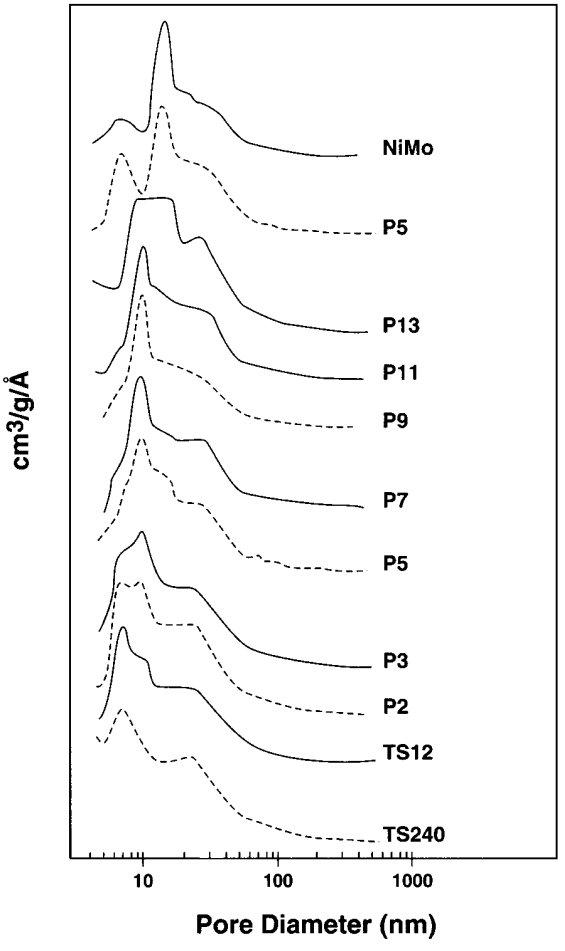

FIG. 10. Pore size distribution of used catalysts with low (top) to high (bottom) carbon content.

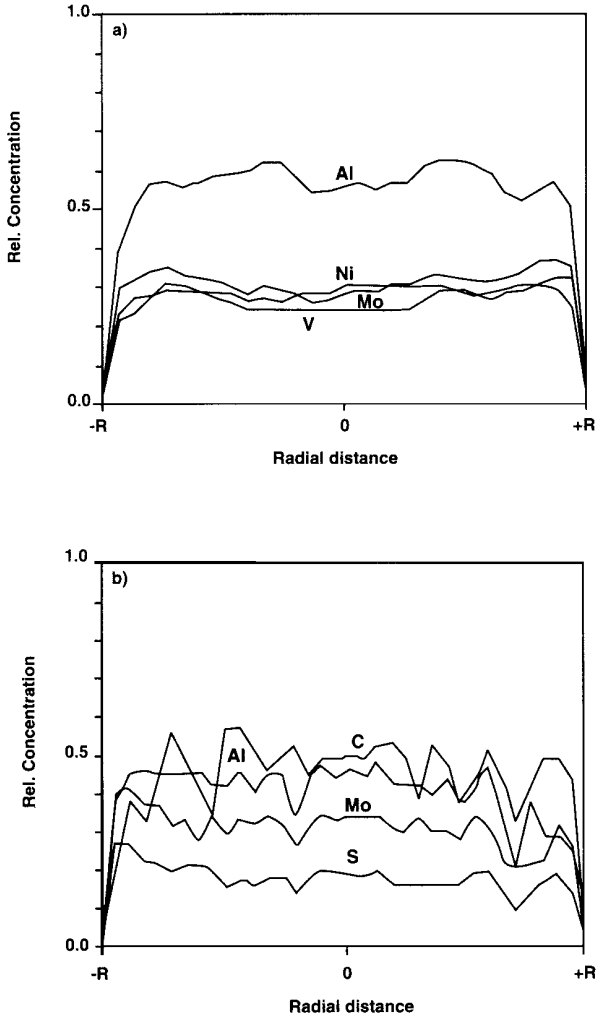

FIG. 12. Vanadium (a) and carbon (b) EPMA radial concentration profile for TS120 (a) and TS240 (b) samples obtained from a continuous flow reactor.

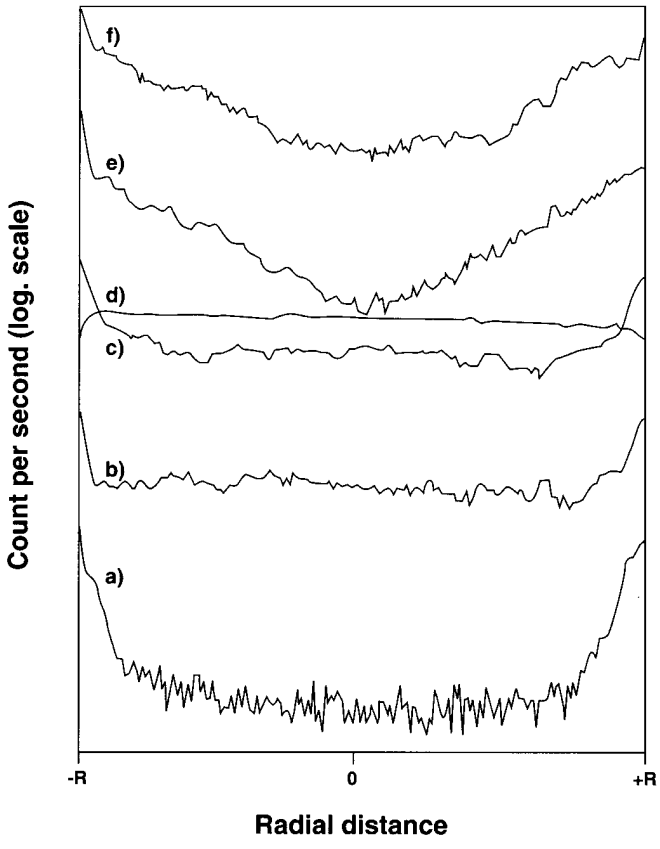

FIG. 13. SIMS carbon radial concentration profiles of used catalysts from the P series obtained from a batch reactor. Samples: (a) NiMo oxide, (b) P15 (4 wt% C), (c) P9 (6.6 wt% C), (d) P9 oxygen signal, (e) P5 (8 wt% C), (f) P2 (10.1 wt% C).

XPS analysis were performed on the used catalysts of the P and TS series which cover the larger range of carbon content. Ni 2p/Al 2p and Mo 3d/Al 2p intensity ratios remained constants at 0.022 and 0.065, respectively, indicating no substantial coverage of the active phase by carbon deposits (54). The S/Mo ratio computed by XPS and reported in Table 4 tends to increase when the carbon content increases. These XPS S/Mo ratio compares well with

TABLE 4

XPS Atomic Ratio for the Used Catalysts from the P and TS Series

Sample	C (wt%)	S (wt%)	S/Mo (XPS)	S/Mo (XRF)
P15	4.0	5.6	1.87	2.03
P9	6.7	6.0	2.30	2.06
P5	8.0	5.6	2.06	2.10
P2	10.1	5.7	2.37	2.28
TS6	11.4	5.6	2.48	2.38
TS72	13.5	5.5	2.54	2.61
TS240	13.7	5.6	2.81	2.85
Presulf-tested	0.6	5.45	2.46	2.11

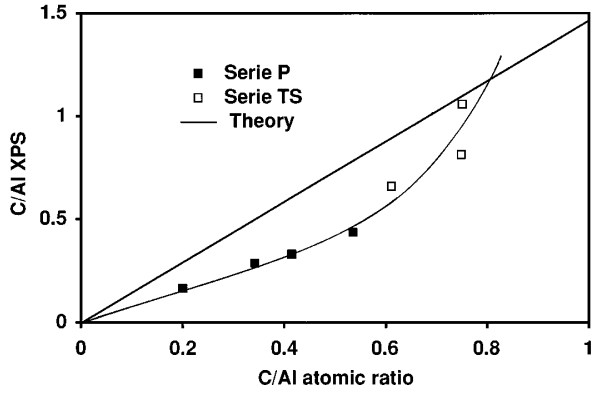

FIG. 14. XPS carbon/aluminum concentration ratio versus carbon content in the form of C/Al atomic ratio.

the S/Mo ratio obtained from XRF as reported in Table 4. As the carbon deposits have been found to contain sulfur it cannot be concluded that the S/Mo ratio of the active phase has changed.

The variation of the intensity ratio C 1s/Al 2p versus the carbon content is plotted in Fig. 14. A linear relationship is found at low carbon content. As the C content reaches 12–14 wt%, the C 1s/Al 2p intensity ratio increases sharply. The theoretical line computed for a perfectly mixed solid (45) is located above the experimental results, suggesting that not all of the carbon is detected by XPS. In other words, the carbon particles should be thick according to the XPS results.

TEM analysis was performed on samples P15 (4.0 wt% C), P2 (10.1 wt% C), TS12 (12.1 wt% C) and TS240 (13.7 wt% C) and some pictures are reported in Figs. 15a to 15d, respectively. These pictures show alumina crystallites and black lines of the MoS_2 layers. From a dozen neat pictures a mean length of the MoS_2 layers has been determined and found to be 6 ± 1 nm. On the TEM pictures, patches of amorphous carbon (granular aspect) can also be distinguished, in particular on the edges of the alumina support zone, as indicated by arrows. The carbon features are similar whatever the carbon content; however, larger areas of the alumina support seem to be covered by amorphous carbon patches as carbon content increases, i.e., the patches tend to be bigger.

Deactivation of used catalysts. A number of samples from the TS and P series were chosen for tests using model compounds in order to evaluate the deactivation of the active phase. Conversions obtained for toluene hydrogenation at 350°C, cyclohexane isomerization into methylcyclopentane at 380 and 400°C, and thiophene hydrodesulfurization at 220°C are reported in Table 5.

The used catalysts were washed with hot toluene after testing with the SAR feed, stored in toluene, and dried before carrying out an activity test with model molecules. Carbon contents were also measured after tests using model

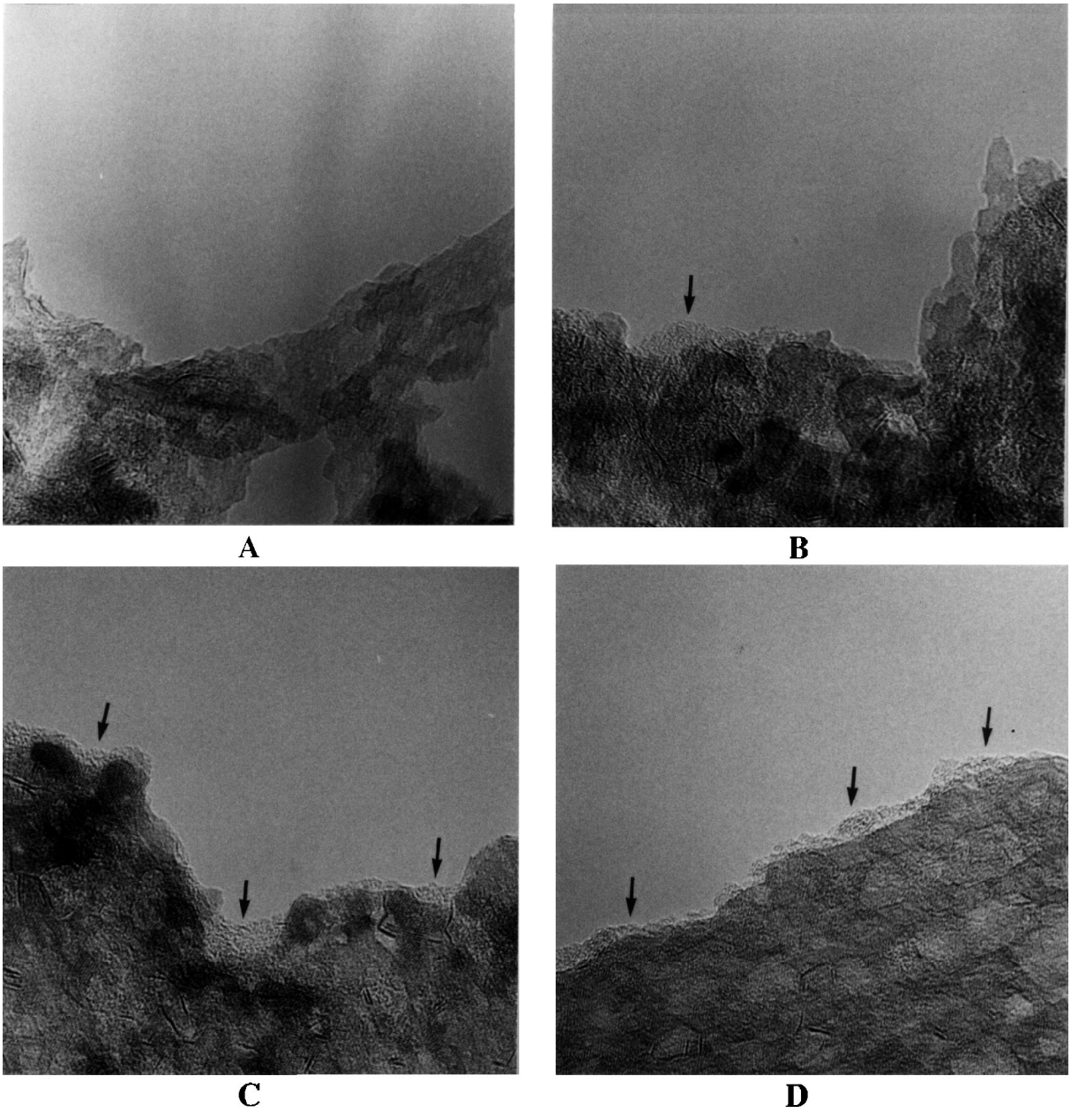

FIG. 15. TEM pictures of used catalysts obtained from a batch reactor (scale, 1 cm = 10 nm). (A) P15 (4 wt% C), (B) P2 (10.1 wt% C), (C) TS12 (12.1 wt% C), (D) TS240 (13.7 wt% C).

molecules to evaluate the possible "decoking effect" of the model feed. The amount of carbon left after model molecules testing is linearly correlated with the initial amount of carbon, with about 40% of the initial carbon being removed (Table 5). It is likely that the carbon loss is due to hydrogenation rather than a washing of the carbon deposits because the used catalysts were soxhlet extracted using toluene prior to analysis and model molecule testing.

To analyze the variation of catalytic activities of the used catalysts, the carbon contents measured on the used samples recovered after tests using model molecules have been considered in the following. As can be noted in Table 5, the cyclohexane isomerization activity at 380 or 400°C is not measurable compared to the activity of the fresh catalyst. As the cyclohexane isomerization is bifunctional in nature, both the poisoning of the hydrogenating function or the acidic function can lead to this effect. However, as the hydrogenation activity is not completely poisoned, the complete poisoning of the isomerization activity strongly suggests that the acid sites are poisoned by the remaining carbon deposits. It is clear from Table 5 that the isomerization activity of the samples containing less than 200 ppm V is also

TABLE 5

Composition and Activities of Used Catalysts Tested with Model Molecules

Sample	C before test (wt%)	C after test (wt%)	V (wt%)	HYD, 350°C (%)	ISOM, 380°C (%)	ISOM, 400°C (%)	HDS, 220°C (%)
NiMo	0.0	1.1	<0.001[a]	37.1	6.3	23.0	41.8
P15	4.0	3.0	0.020[a]	13.5	<0.2	<0.2	33.7
P13	5.0	3.4	0.020[a]	10.8	<0.2	<0.2	34.8
P9	6.7	4.7	0.020[a]	5.8	<0.2	<0.2	30.6
P5	8.0	5.3	0.019[a]	5.7	<0.2	<0.2	32.8
P2	10.1	6.1	0.018[a]	4.0	<0.2	<0.2	29.8
TS6	11.4	5.8	0.06[b]	3.2	<0.2	<0.2	32.7
TS120	13.7	8.8	0.77[b]	0.8	<0.2	<0.2	16.0
TS240	13.7	9.6	1.3[b]	0.4	<0.2	<0.2	10.3

[a] Computed from HDV on a fresh catalyst basis.
[b] Measured by X-ray Fluorescence.

poisoned, indicating that the catalyst acidity has been considerably neutralized by the carbon deposits rather than by the V deposits.

From the HYD and HDS conversions, first-order HYD and HDS activities have been computed and plotted in Fig. 16 versus the carbon content and in Fig. 17 versus the vanadium content. In batch reactor a maximum amount of 203 ppm V can be deposited on the catalyst. For the series of samples obtained by varying the pressure (P series), the HDV varies between 89 and 99% and therefore the amount of V deposited onto the catalyst increases from 180 to 200 ppm, i.e., can be considered to remain constant. In parallel, the carbon content varies from 4 to 10 wt%; hence in Fig. 16 the plot of the HYD and HDS activities for the P series versus the carbon content is relevant to the deactivating effect of the carbon deposits. It can be seen that this deactivating effect is more important on the HYD than on the HDS function.

In the continuous flow tests (TS series), the amount of V deposited varies in a large range, from 0.06 to 1.3 wt%

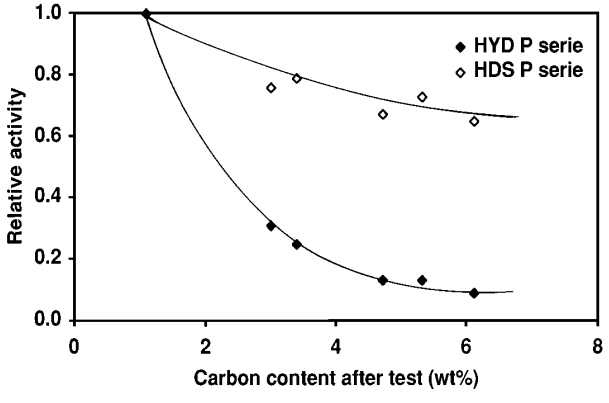

FIG. 16. Toluene HYD and thiophene HDS versus carbon content of the P series of used catalysts obtained from a batch reactor.

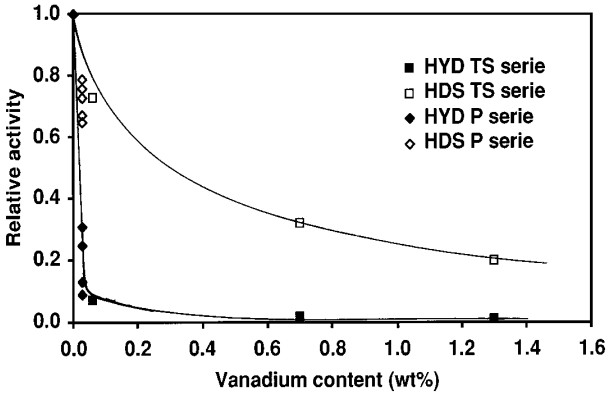

FIG. 17. Toluene HYD and thiophene HDS versus vanadium content of the TS series obtained from a continuous flow reactor.

with the V well dispersed in the catalyst grains, whereas the amount of carbon remains between 11 to 14 wt%. Thus the plot in Fig. 17 of the relative activities of the used catalysts from the TS series versus the vanadium content is relevant to the deactivating effect of vanadium especially in the case of the HDS function, whereas the very low hydrogenation activity of high C and V content catalysts make the comparison difficult for the HYD function. It can also be observed in Fig. 17 that the HYD is much more strongly poisoned than the HDS function.

DISCUSSION

The batch and continuous flow reactor tests performed with the SAR feed in this work were designed to produce used catalysts from a real feed operation containing only minor amounts of metal deposits. In doing so it was expected that the role of the carbon and metal deposits in the initial deactivation of a residue hydrotreating catalysts would be more easily identified. Used catalysts with amounts of carbon ranging between 4 and 15 wt% and less than 200 ppm V were obtained from batch reactor experiments and samples with less than 1.3 wt% of vanadium and 11 to 14 wt% C were obtained in a continuous flow reactor.

The results reported in this work confirm that the carbon deposits are not irreversible species neither in terms of composition nor in terms of quantity. Note that the carbon deposits in this work have to be considered as being initial deposits or "young coke" because the time on stream or contact time employed were short compared to industrial operations. The behavior of the carbon deposits is clearly dynamic and depends on the operating conditions as well as the nature of the feed.

The rather high level of carbon content obtained from the tests in continuous flow reactor at a rather low pressure for a residue HDM operation is not surprising. The process of carbon deposition onto hydroprocessing catalyst is known to be rapid and the results of Fig. 2 indicate

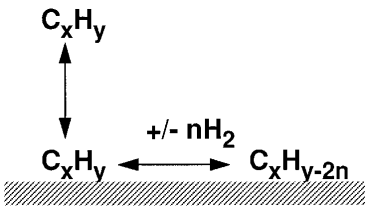

SCHEME I

that in our experimental conditions the carbon deposition is extremely rapid. The decrease of the H/C ratio versus time on stream indicates the evolution of the coke to a more dehydrogenated form as the time on stream increases. This effect is known and is often assumed to be a slow evolution or aging of the coke deposits versus time.

In a batch reactor the effect of increasing the pressure is a decrease in the amount of carbon and an increase in the hydrogen content of the carbon deposit as often reported. More surprising is the influence of increasing the contact time, which led to a decrease in the carbon content. This result indicates that the hydrocarbon phase is more and more purified as the contact time increases in batch reactor; hence, there is a lower concentration of coke precursor in the feed and even desorption of hydrogenated coke components, which leads to a decrease in the carbon content of the used catalyst. The simple reaction Scheme I describes the equilibrium between feed coke precursor and surface coke precursors with n the extent of dehydrogenation.

Noticeably, the amounts of carbon deposited onto the catalysts in continuous flow reactor are always higher than the amounts deposited in a batch reactor. This indicates that in a continuous flow reactor the fresh feed constantly brings new coke precursors and hence tends to displace the surface equilibrium toward more surface carbon and in a more dehydrogenated form. The results of the batch reactor tests indicate, therefore, that the carbon deposits can be reversibly hydrogenated and desorbed, at least in part.

The effect of the reaction temperature in a batch reactor led to the same conclusion. Usually, the amount of coke increases and the H/C ratio decreases when the reaction temperature increases as the dehydrogenation reactions are favored. However, in a batch reactor, an increase in reaction temperature led also to an increased purification of the feed, hence favoring hydrogenation and desorption of coke precursors at least up to 400°C. At higher temperatures, the dehydrogenation of the coke prevails. In other words, in a batch reactor the coking propensity of the feed decreases when hydropurification increases, i.e., when pressure, temperature, and contact time increase. In a continuous flow reactor the coke propensity of the feed remains constant, hence the accumulation of carbon deposits.

The reversibility of at least part of the carbon deposits is also observed when the catalyst is compared with the alumina support. The used support contains much more carbon than the catalyst for the same operating conditions and feed. This shows that the active phase plays a role through the hydropurification of the feed and in particular by hydrogenation of the coke precursors and carbon deposits. Thus the active phase moderates the carbon deposition as expected (49).

The role of the acidity of the catalyst has been emphasised many times in the literature. The effect of fluorine found in this work is not conclusive, whereas the effect of Na is clear, suggesting that the acidic sites of the alumina support are the adsorption sites of coke precursors and/or the "sitting sites" of carbon deposits.

In this work, all of the used samples were obtained from the same NiMo catalyst, except those prepared with the alumina support. It was therefore tempting to seek more general correlations concerning the elemental composition of the used catalysts. As a matter of fact, the set of used catalysts obtained in this work appears remarkably consistent. The coke deposits appear to have, within the experimental uncertainties, the same general features such as the same sulfur and nitrogen content (Figs. 6 and 7), the same coke bulk density as found for the used catalyst bulk density versus carbon content correlation (Fig. 9), and the same morphology with a mean mesopore diameter versus carbon content correlation (Fig. 10). However, differences in composition exist as indicated by the variation of the H/C ratio with the carbon content (Fig. 8).

The sulfur content of the used catalysts increases slightly when the amount of carbon increases as shown in Fig. 6. The main contribution to the sulfur content of the used catalyst is the sulfide active phase and such an effect can be due either to the presence of sulfur in the carbon deposits and/or an increase of the sulfidation state of the NiMo sulfide active phase. Recent studies using temperature programmed oxidation have shown that indeed the coke in used hydroprocessing catalysts contain some sulfur (55–59). As a matter of fact, the sulfided alumina support retains only a negligible amount of sulfur, whereas the coked alumina support does contain some sulfur with the same S/C ratio (S/C = 0.035) as the used NiMo catalysts (Table 2). Thus, although the presence of the active phase should lead to a more desulfurized carbon deposit, it appears that within the experimental errors the carbon deposits in the used catalyst contain sulfur with a S/C atomic ratio of 0.035 ± 0.01.

From the sulfur contents of the used catalysts, the S/metal atomic ratio can be computed and is found between 1.4 and 1.6. This ratio being lower than 2, it indicates that the active NiMo phase is sulfur deficient in the experimental conditions employed.

The used catalyst contains somewhat higher nitrogen content than the coked alumina support, which suggests that the NiMo sulfide active phase adsorb some nitrogen containing species, as demonstrated in Ref. 59.

The H/C atomic ratio of the used catalyst decreases monotonously when the carbon content increases as shown in Fig. 8. Although this tendency may be fortuitous it may also suggest that the hydrogen content of the carbon deposits not only depend on the operating conditions and in particular pressure, temperature, and age but also on the carbon content. This can be understood by a surface equilibrium between more or less hydrogenated form of the carbon deposits as shown in Scheme I. From Scheme I the relationship between the H content and the C content can be computed (see Appendix II) and indeed a linear relationship (formula [II.6]) is found.

Formula II.6 indicates also that, within the hypothesis made, the concentration of coke precursor will influence the amount of carbon deposited hence the H/C ratio, whereas the hydrogen pressure will not influence the H/C ratio at constant carbon content. This later observation must be moderated because only one surface carbon species has been taken into account in Scheme I and in the calculation in Appendix II, whereas if several surface intermediates at different stage of dehydrogenation are taken into account, the hydrogen pressure will influence the proportion of these dehydrogenated surface species and hence the H/C ratio. In addition, the coke is likely of the same type, i.e., "young coke" in our study, and it is not yet deeply transformed by ageing.

The range of carbon deposit density is limited and this result appears to be notably different from results obtained on used reforming catalysts where the coke density is always notably different when operating conditions change (60). X-ray diffraction as well as TEM analysis indicate no formation of highly structured carbon phase like graphitic or pregraphitic carbon. TEM analysis suggests the existence of large patches of amorphous carbon covering only part of the alumina surface. This is in agreement with the XPS data suggesting that these patches have a large thickness as the C/Al XPS ratio is lower than the calculated value for a perfectly mixed solid. The 1.15 ± 0.2 g/cm^3 density range is typical of tri- or polyaromatics or asphaltens (10) more or less hydrogenated and it can be suggested that the carbon deposits are generated from asphaltens and polyaromatic adsorption with some polymerization or aggregation on the surface and dehydrogenation depending on the experimental conditions.

The net decrease of the mean pore diameter (17 to 3 nm) with the amount of carbon deposit, an often reported phenomenon (2, 5, 12, 21, 61, 62), is clearly demonstrated in this work for a residue HDM catalyst and suggests also that the carbon particles have a large thickness. This can be verified by a simple calculation. If the carbon is deposited in the form of a uniform layer covering the catalyst surface, the 15% of the total pore volume or 28% of the mesopore volume occupied by 14 wt% carbon with a bulk density of 1.15 g/cm^3 corresponds to a layer of about 15% the mean mesopore diameter, i.e., 2.5 nm for a cylindrical pore model. As the mean mesopore diameter decreased by 14 nm, this indicates that the carbon deposits are not likely in the form of a uniform layer covering all of the surface area but rather in the form of three-dimensional particles (63).

The mean pore size of about 3 nm determined for the 14 wt% carbon sample was therefore generated by the growth of carbon particles or patches with a height of about 14 nm which then creates pore restriction of a small size. Taking 14 nm as the mean height of the carbon particle, it can be easily computed that the surface covered by the carbon particles is about 28% of the total surface area. This is quite a high proportion, indicating that carbon particles are either numerous but small in lateral size or in small amount and very large. Considering a cube of 14 nm as a model of the small carbon particle, one can compute that 1.5×10^{15} cubic carbon particles are spread out over 1 m^2 of the alumina surface. Considering now patches of $140 \times 140 \times 14$ nm, a value of 1.5×10^{13} carbon particles/m^2 is found.

While the length of the carbon particles cannot be exactly determined, these results suggest a model of amorphous, nongraphitic, three-dimensional particles for the part of the carbon deposits visible by TEM (63). It must be noted that this description is valid for young carbon deposits as our tests lasted only a short time. Evolution toward more structured carbon deposits upon aging is likely as suggested in the literature (48, 61, 62).

The almost uniform distribution of vanadium and carbon in the grain indicates that diffusional limitations were not operating during the preparation of most of the used catalysts samples studied in this work with the exception of the samples prepared in a batch reactor at very low pressure and containing high carbon content, showing a U-shaped profile for the radial carbon concentration profile. Therefore the real deactivating effect of C and V on the active phase can be determined.

The carbon deposits are shown in Fig. 16 to deactivate the active phase in absence of metal deposits (batch samples). This indicates that either the number of the active sites or their reactivity has decreased. To investigate the various hypothesis concerning the deactivating effect of carbon on the active phase, it is of interest to compare the number of carbon atoms deposited per MoS_2 slab. The description of the molybdenum disulfide particles as regular hexagonal single slabs well dispersed over the alumina support surface permits calculations of the number of molybdenum ion per MoS_2 slab and of the number of slabs per nm^2 of surface area for the 8.4 wt% Mo containing catalyst (64). Taking a MoS_2 slab size of 5 nm to obtain a regular hexagonal slab model containing 169 Mo ions, a surface density of 2.7×10^{16} slab/m^2 is found (Table 6).

It can be seen in Table 6 that a large number of carbon atoms is deposited per MoS_2 slab for a 10 wt% C loading. When considering the number of carbon particles pre-

TABLE 6

Comparison of Surface Densities of V, C, and MoS_2 Slabs for a Used Catalyst Containing 200 ppm V or 1 wt% V, and 10 wt% C

Catalyst composition	
Mo at./nm^2 (8.4 wt% Mo)	4.6
V at./nm^2 (200 wt ppm V)	0.02
V at./nm^2 (1 wt% V)	1.0
C at./nm^2 (10 wt% C)	44
MoS_2 slab model (64)	
Slab size in nm	5
Mo at./slab (M)	169
Edge Mo at./slab (Me)	36
Me/M	0.21
MoS_2 slab/nm^2	0.027
V at./slab (200 ppm V)	0.74
V at./slab (1 wt% V)	37
C at./slab (10 wt% C)	1630

viously computed, one can find that there are about 20 MoS_2 slabs for every 14 nm^3 carbon patch, whereas there are 1800 MoS_2 slabs for every $140 \times 140 \times 14$ nm carbon patch. If one assumes that a carbon particle covers one slab, this calculation shows that only a very limited amount of MoS_2 slab will be inactive and this cannot explain the deactivation observed. If one considers now that the carbon patches grows from the edge of the MoS_2 slabs and therefore poison a few active edge sites then only a very small amount of sites will be poisoned. It could also be argued that the growth of the carbon patches from a site of a MoS_2 slab induces an interaction between the MoS_2 slab and the carbon particle that can decrease the reactivity of the slab. However, the number of slab being much larger than the number of carbon particles this cannot lead to the deactivation observed. Therefore, there must be another explanation such as the presence of carbonaceous moieties on the edges of the MoS_2 slabs or an electronic effect of the carbon deposits that perturbs all of the MoS_2 slabs on the alumina surface as indicated by the change of the HYD/HDS selectivity. While our results do not allow discrimination between these two hypotheses, it is worth noting that there is a very large amount of carbon per MoS_2 slab and therefore it is possible that all of the slabs possess some surface carbon which will poison some sites and eventually modify the reactivity of the free sites remaining.

While the carbon deposits deactivate the catalyst, it appears from the tests of the used catalysts using model reactants that a small amount of vanadium deposits deactivate even more efficiently the catalyst. This is particularly observed in Fig. 17 for the HDS function which is more deactivated by 1.3 wt% V than by 14 wt% C. This conclusion can be drawn because the small amount of vanadium deposited is almost uniformly distributed in the grain volume. A vanadium radial concentration gradient induced by a diffusion limitation may be one reason for the discrepancies found in the literature. In such cases, the active phase inside the grain is less affected by the vanadium.

The initial poisoning of the active phase by metals for real feed tests have been already invoked by several authors (19, 23, 30). The observation of a strong poisoning of the NiMo active phase by vanadium has been mainly demonstrated in model compound studies (35–37, 39). Several possibilities can be considered to explain this deactivation such as a substitution of the Ni by V in the NiMoS active phase according to the schematic reaction (39, 65)

$$\mathrm{NiMoS} + \mathrm{VS} \rightarrow \mathrm{VMoS} + \mathrm{NiS} \qquad [4]$$

or captation of the Ni by the vanadium sulfide VS deposits (41) according to the schematic reaction

$$\mathrm{NiMoS} + \mathrm{VS} \rightarrow \mathrm{MoS} + \mathrm{NiVS} \qquad [5]$$

or destabilization of the NiMoS phase according to the schematic reaction

$$\mathrm{NiMoS} + \mathrm{VS} \rightarrow \mathrm{MoS} + \mathrm{NiS} + \mathrm{VS} \qquad [6]$$

In all cases, destruction of the NiMoS phase occurs and the large promoting effect of Ni is lost. If a VMoS phase is formed, only a very limited promoting effect will be generated compared to Ni promotion (65).

To illustrate these possibilities, the surface densities of vanadium have been computed in Table 6 for two V loadings: 200 ppm and 1 wt%. A 200 ppm V loading calculates to 0.74 V atom per 5 nm MoS_2 slab containing 36 edge Mo ions. Thus 200 ppm V is not sufficient to poison the active phase particles of the catalyst. For a 1 wt% V loading, 37 V atoms are deposited per 5 nm MoS_2 slab containing 36 edge Mo ions. In this case the number of vanadium per MoS_2 slab approaches the number of edge sites and complete promoter ion substitution appears possible for a 1 wt% V loading with 100% dispersion on the MoS_2 slab edges.

Another deactivation mechanism is the coalescence of the MoS_2 active phase leading to the loss of active surface area as proposed by Smith and Wei (43). However, this mechanism does not appear to be effective in our conditions where only very small amounts of V have been deposited as TEM studies show no clear indication of sintering of the active phase.

Carbon and metal deposits influence the HYD/HDS balance as shown in Figs. 16 and 17 with the HYD being more strongly poisoned than the HDS in both cases. Evidence for a change in the HYD/HDS balance of sulfided hydrotreating catalysts when various parameters are changed such as operating conditions and sulfiding conditions are numerous in the literature. For example, the sulfiding temperature has been found to influence notably the HYD/HDS balance (66–68). Such results are often interpreted by the existence of two different catalytic sites. However, in general, the

HYD and HDS functions are not probed under the same conditions and in particular at same reaction temperature. Another interpretation is that HYD and HDS proceed by two different rate determining steps that do not require the same active surface species (69), although the reactants are adsorbed on similar sites. Whatever the interpretation, this change in the selectivity strongly suggests that there is a chemical perturbation of the active phase by both carbon and V rather than only a site blockage.

It appears therefore that the mode of deactivation of each of the deactivating agents, C or V, can be notably different. While it can be suggested that vanadium deactivates the catalyst by destabilization of the NiMoS phase or by captation of the Ni promoter (35–37, 39, 65), it is likely that some surface carbon species on the MoS_2 slab edges are responsible for the deactivation, although most of the carbon accumulates in large particles in interaction with the support surface, neutralizing in particular the acidic sites.

The results reported in this work indicate that both carbon and metals deposits deactivate the catalyst as previously reported (70). However, our results suggest that metal deactivation predominates over carbon deactivation. While this is observed at the initial stage of the deactivation process or of the run of the hydrotreater, at a more advanced stage, the effect of each deposit becomes even more complex. The carbon particles and the vanadium sulfide particles grow (41) and generate pore size restrictions that can generate diffusional limitations in particular for the vanadium deposition. In addition, coalescence of the active phase can also occur, leading to loss of activity (43), whereas vanadium sulfide, also active for the various hydrotreating reactions (40, 71) will bring some activity. Hence the interplay between carbon deposits, vanadium sulfide deposit, and the active phase is likely to be different at the initial, intermediate, and final deactivation periods of a residue HDM catalyst.

CONCLUSION

The present study has shown that in a continuous flow reactor both carbon and metals are deposited on the catalyst with carbon content reaching very quickly a steady-state concentration and with higher amounts than in a batch reactor. Used catalyst composition analysis indicates that the carbon deposits contain sulfur, nitrogen, and hydrogen with hydrogen content depending on the experimental conditions and the amount of carbon deposited. The variation of the carbon content with pressure, temperature, and contact time demonstrates the dynamic nature of the carbon deposits regulated by reversible hydrogenation–dehydrogenation reactions. Characterization studies have shown that V and C were well distributed in the catalyst grain in most of the samples and that the major type of carbon deposits present were three-dimensional amorphous carbon patches with a 1.15 ± 0.2 g/cm^3 bulk density. Some carbon species have a deactivating effect on both the HYD and the HDS functions and the change of the HYD/HDS selectivity vs carbon content of vanadium free samples suggests that there are some carbonaceous species on the active phase surface. The deactivation by vanadium is attributed to a destruction of the NiMoS phase and the loss of the promoter effect of Ni on the MoS_2 phase. It is concluded that when metals and carbon are uniformly deposited in the particle of a bimodal macroporous hydrodemetallization catalyst, both contribute to the deactivation but with metal deactivation predominating over coke deactivation at the very beginning of a run of a resid hydrotreater.

APPENDIX I

The relationship between the bulk density and the carbon content of the used catalysts can be computed as follows (60). For the fresh catalyst the bulk density ds as measured by helium picnometry is

$$\mathrm{ds} = \frac{m}{V}, \qquad [\mathrm{I.1}]$$

and the total pore volume, TVP, is

$$\mathrm{TPV} = \frac{v}{m}, \qquad [\mathrm{I.2}]$$

with m, V, and v representing the mass, volume of matter, and pore volume of fresh catalyst, respectively. For the used catalyst, the carbon content, C in wt%, is

$$C = 100\frac{m_c}{m + m_c}, \qquad [\mathrm{I.3}]$$

the coke density is

$$\mathrm{ds_c} = \frac{m_c}{v_c}, \qquad [\mathrm{I.4}]$$

the bulk density measured by helium picnometry is

$$\mathrm{ds_u} = \frac{m + m_c}{V + v_c}, \qquad [\mathrm{I.5}]$$

and the total pore volume is

$$\mathrm{TPV_u} = \frac{v_{ac}}{m + m_c}, \qquad [\mathrm{I.6}]$$

with m_c the carbon content, v_c the volume occupied by the carbon, and v_{ac} the accessible volume. From relationships [I.1] to [I.6] it can be found that the density and carbon content of a used catalyst are related by the equation

$$\frac{1}{\mathrm{ds_u}} = \frac{1}{\mathrm{ds}} + \left(\frac{1}{\mathrm{ds_c}} - \frac{1}{\mathrm{ds}}\right)C, \qquad [\mathrm{I.7}]$$

which leads to a straight line if the coke density is constant. If there is some occluded volume v_{oc} then

$$v = v_c + v_{ac} + v_{oc} \qquad [I.8]$$

and the bulk density of the used catalyst is

$$ds_u = \frac{m + m_c}{V + v_{ac} + v_{oc}}. \qquad [I.9]$$

It can then be established that

$$\frac{1}{ds_u} = \frac{1}{ds} + \frac{v_{oc}}{m} + \left(\frac{1}{ds_c} - \frac{1}{ds} - \frac{v_{oc}}{m}\right)C, \qquad [I.10]$$

which gives a linear relationship if the occluded volume as well as the coke density remain constants. If the coke density is constant, then the occluded volume is written:

$$v_{oc} = m \cdot TPV - \frac{TPV_u}{1 - C} - \frac{C}{(1 - C)ds_c}. \qquad [I.11]$$

APPENDIX II

To compute the relationship between the H/C ratio and the C content, the simple reaction model described in Scheme I is used with a surface containing one type of site symbolized by $*$. The two equilibrated reactions corresponding to Scheme I can be written as

$$C_xH_y + * \leftrightarrow *\text{-}C_xH_y \qquad K_C \qquad [II.1]$$

$$*\text{-}C_xH_y \leftrightarrow *\text{-}C_xH_{y-2n} + nH_2 \qquad K_{DHYD}, \qquad [II.2]$$

with K_C and K_{DHYD} the equilibrium constant for the adsorption of the coke precursor C_xH_y and for the equilibrated dehydrogenation reaction, respectively. The site, carbon, and hydrogen balance equations are written as

$$[*]_o = [*] + [*\text{-}C_xH_y] + [*\text{-}C_xH_{y-2n}] \qquad [II.3]$$

$$[C] = x([*\text{-}C_xH_y] + [*\text{-}C_xH_{y-2n}]) \qquad [II.4]$$

$$[H] = y[*\text{-}C_xH_y] + (y - 2n)[*\text{-}C_xH_{y-2n}], \qquad [II.5]$$

with $[*]_o$ the initial site concentration. From these relationships, the dependence of the hydrogen concentration with the carbon content can be obtained by eliminating K_{DHYD}, and one obtains

$$[H] = 2nK_CP_C[*]_o + \frac{1}{x}(y - 2n(1 + K_CP_C))[C], \qquad [II.6]$$

where P_C is the concentration of the coke precursor C_xH_y.

ACKNOWLEDGMENTS

We are indebted to the staff of the Division physicochimie et analyses of IFP for their efforts in performing the elemental analysis, TEM, XPS, and EPMA analysis, to C. Russmann and H. Ajot for textural analyses, to Eurecat S. A, La Voulte-sur-Rhône, France, for the *ex situ* presulfiding of the catalyst, to J. Lynch and the staff of 'Sciences et Surface SA' for the SIMS analysis, and to H. Toulhoat for the initialization of this work.

REFERENCES

1. Ohtsuka, T., *Catal. Rev. Sci. Eng.* **16**, 291 (1977).
2. Beuther, H., and Schmid, B. K., "Proceedings, 6th World Petroleum Congress," Section III, paper 20, 1963.
3. Ternan, M., Furimsky, E., and Parson, B. I., *Fuel Proc. Tech.* **2**, 45 (1979).
4. Togari, O., Takahashi, H., and Nakamura, M., *J. Jpn. Petrol. Inst.* **23**, 256 (1980).
5. Beuther, H., Larson, G. A., and Perrotta, A. J., *Stud. Surf. Sci. Catal.* **6**, 271 (1980).
6. Ternan, M., and Kriz, F., *Stud. Surf. Sci. Catal.* **6**, 283 (1980).
7. Hegedus, L. L., and McCabe, L. L., *Stud. Surf. Sci. Catal.* **6**, 471 (1980).
8. Delmon, B., and Grange, P., *Stud. Surf. Sci. Catal.* **6**, 507 (1980).
9. Sie, S. T., *Stud. Surf. Sci. Catal.* **6**, 545 (1980).
10. Speight, J. G., "The Desulfurization of Heavy Oils and Residua." Dekker, New York, 1981.
11. Galiasso, R., Blanco, R., Gonzales, C., and Quinteros, N., *Fuel* **62**, 817 (1983).
12. Thakur, D. S., and Thomas, M. G., *Appl. Catal.* **15**, 197–225 (1985).
13. Shimura, M., Shiroto, Y., and Kakeuchi, C., *IEC Fundam.* **25**, 330 (1986).
14. Ammus, J. M., Androutsopoulos, G. P., and Tsetsekou, A. H., *IEC Res.* **26**, 1312 (1987).
15. Pereira, C. J., Donnelly, R. G., and Hegedus, L. L., *in* "Catalyst Deactivation" (E. E. Petersen and A. T. Bell, Eds.), Vol. 30, Chap. 12, p. 315. Dekker, New York, 1987.
16. Wei, J., *in* "Catalyst Design, Progress and Perspectives" (L. L. Hegedus, Ed.), p. 245. Wiley, 1987.
17. Quann, R. J., Ware, R. A., Hung, C., and Wei, J., *Adv. Chem. Eng.* **14**, (1988).
18. Trimm, D. L., *Stud. Surf. Sci. Catal.* **53**, 41 (1989).
19. Bridge, A. G., *Stud. Surf. Sci. Catal.* **53**, 363 (1989).
20. Wei, J., *Stud. Surf. Sci. Catal.* **68**, 333 (1991).
21. Absi-Halabi, M., Stanislaus, A., and Trimm, D. L., *Appl. Catal.* **72**, 193 (1991).
22. Bartholomew, C. H., *in* "Catalytic Hydroprocessing of Petroleum and Distillates," Chemical Vol. 51, p. 1. Dekker, New York, 1994.
23. Tamm, P. W., Harnsberger, H. F., and Bridge, A. G., *IEC Prod. Des. Dev.* **20**, 262 (1981).
24. Hannerup, P. N., and Jacobsen, A. C., *Preprint ACS, Div. Petrol. Chem.* **28**(3), 576 (1983).
25. Dautzenberg, F. M., Van Klinken, J., Pronk, K. M. A., Sie, S. T., and Wijffels, J. B., *ACS Symp. Ser.* **65**, 254 (1978).
26. Newson, E., *IEC Prod. Des. Dev.* **14**, 27 (1975).
27. Inoguchi, M., Kagaya, H., and Daigo, K., *Bull. Jpn. Petrol. Inst.* **13**, 153 (1971).
28. Stohl, F. V., Stephens, H. P., Stiegel, G. J., and Tischer, R. E., *EPRI Cong.* AP-3825-SR (1985).
29. Delmon, B., *Appl. Catal.* **15**, 1 (1985).
30. Johnson, B. J., Massoth, F. E., and Bartholdy, J., *AIChE J.* **66**, 505 (1986).
31. Rajagopalan, K., and Luss, D., *IEC Prod. Des. Dev.* **18**, 459 (1979).
32. Kang, S. J., and Mosby, J. F., *IEC Prod. Des. Dev.* **25**, 437 (1986).
33. Makarenko, I. V., Rodjkin, S. P., and Lipovich, V. G., *Neftekhimiya* **24**, 209 (1984).
34. Bartholdy, J., Zeuthen, P., and Cooper, B. H., "Preprints, AIChE Spring National Meeting," paper 56c, 1994.
35. Mitchell, P. C. H., *Catal. Today* **7**, 439 (1990).

36. Mitchell, P. C. H., and Scott, C. E., *Catal. Today* **7**, 467 (1990).
37. Ledoux, M. J., Hantzer, S., Panissod, P., Petit, P., André, J., and Callot, H. J., *J. Catal.* **106**, 525 (1987).
38. Ledoux, M. J., and Hantzer, S., *Catal. Today* **7**, 479 (1990).
39. Dejonghe, S., Hubaut, R., Grimblot, J., Bonnelle, J. P., DesCourières, T., and Faure, D., *Catal. Today* **7**, 569 (1990).
40. Bonné, R. L. C., van Steenderen, P., and Moulijn, J. A., *Bull. Soc. Chim. Belg.* **100**, 877 (1991).
41. Toulhoat, H., Szymanski, R., and Plumail, J. C., *Catal. Today* **7**, 531 (1990).
42. Smith, B. J., and Wei, J., *J. Catal.* **132**, 1 (1991).
43. Smith, B. J., and Wei, J., *J. Catal.* **132**, 21 (1991).
44. Berrebi, G., and Roumieux, R., *Bull. Soc. Chim. Belg.* **96**, 967 (1987).
45. Kerkhoff, F. P. J. M., and Moulijn, J. A., *J. Phys. Chem.* **83**, 1612 (1979).
46. Scofield, J. H., *J. Electr. Spectrosc. Relat. Phenom.* **8**, 129 (1976).
47. Van Dongen, R. H., Bode, D., Vandereijk, H., and Van Klinken, J., *IEC Proc. Des. Dev.* **19**, 630 (1980).
48. Alvarez, D., Galiasso, R., and Andreu, P., *J. Jpn. Petr. Inst.* **22**, 234 (1979).
49. de Jong, K. P., Reinalda, D., and Emeis, C. H., *Stud. Surf. Sci. Catal.* **88**, 155 (1994).
50. Veluswamy, L. R., Ph.D. thesis, Univ. of Utah (1977).
51. Stephens, H. P., and Kottenstette, R. J., *Preprint ACS, Div. Fuel Chem.* **30**(2), 345 (1985).
52. Shabtai, J., Veluswamy, L. R., and Oblad, A. G., *Preprint ACS, Div. Fuel Chem.* **23**(1), 107 (1978).
53. Frozard, P. R., McMillan, J. W., and Zeuthen, P., *J. Catal.* **152**, 103 (1995).
54. deJong, K. P., Kuipers, H. P. C. E., and van Veen, J. A. R., *Stud. Surf. Sci. Catal.* **68**, 289 (1991).
55. Massoth, F. E., and Zeuthen, P., *J. Catal.* **145**, 216 (1994).
56. Wukash, J. E., and Rase, H. F., *IEC Prod. Des. Dev.* **21**, 558 (1982).
57. Furimsky, E., *Erdöl Und Kohle Erdgas,* 455 (1982).
58. Zeuthen, P., Blom, P., and Massoth, F. E., *Appl. Catal.* **78**, 265 (1991).
59. Zeuthen, P., Blom, P., Muegge, B., and Massoth, F. E., *Appl. Catal.* **68**, 117 (1991).
60. Espinat, D., Freund, E., Dexpert, H., and Martino, G., *J. Catal.* **126**, 496 (1990).
61. Butt, J. B., *Adv. Chem. Series* **109**, 259 (1972).
62. Wolf, E. E., and Alfani, F., *Catal. Rev. Sci. Eng.* **24**, 329 (1982).
63. van Doorn, J., and Moulijn, J. A., *Fuel Proc. Tech.* **35**, 275 (1993).
64. Kasztelan, S., Toulhoat, H., Grimblot, and J., Bonnelle, J. P., *Appl. Catal.* **13**, 127 (1984).
65. Mitchell, P. C. H., and Valero, J. A., *React. Kinet. Catal. Lett.* **20**, 219 (1982).
66. Breysse, M., Cattenot, M., Decamp, Th., Frety, R., Gachet, Ch., Lacroix, M., Leclercq, Ch., de Mourgues, L., Portefaix, J. L., Vrinat, M., Houari, M., Kasztelan, S., Bonnelle, J. P., Housni, S., Bachelier, J., and Duchet, J. C., *Catal. Today* **4**, 39 (1988).
67. Candia, R., Sorensen, O., Villadsen, J., Topsoe, N. Y., Clausen, B. S., and Topsoe, H., *Bull. Soc. Chim. Belg.* **93**, 763 (1984).
68. Prada-Silvy, R., Beuken, J. M., Bertrand, P., Hodnett, B. K., Delannay, F., and Delmon, B., *Bull. Soc. Chim. Belg.* **93**, 775 (1984).
69. Kasztelan, S., *Preprints, Div. Petr. Chem., ACS* **38**(3), 642 (1993).
70. Kim, S., and Massoth, F. E., *Fuel Proc. Tech.* **35**, 289 (1993).
71. Takeuchi, C., Asaoka, S., Nakata, S. I., and Shiroto, Y., *Preprints, Div. Petr. Chem., ACS,* **30**, 96 (1983).